Valley-mixing effects in $(GaAs)_l(AlAs)_m$ superlattices with microscopically imperfect interfaces

I. Morrison, L. D. L. Brown, and M. Jaros
Department of Physics, The University of Newcastle upon Tyne, Newcastle upon Tyne NE1 7RU, United Kingdom
(Received 6 August 1990)

We report the first full-scale calculation of the subband structure along the cubic axes of GaAs-AlAs superlattices with microscopically imperfect interfaces. We show that the valley-mixing effects can be used as a sensitive probe of the interface disorder whose characteristic dimension is of order of the bulk lattice constant. It would appear that our predictions concerning the effect of disorder on the optical spectra of small-period structures are in close agreement with recent experimental data.

I. INTRODUCTION

Advances in molecular-beam-epitaxy techniques enable semiconductor interfaces to be grown with near monolayer accuracy.[1,2] The identification of a microscopic signature of interface quality remains one of the most outstanding issues of solid-state physics. In direct-band-gap semiconductor microstructures exciton recombination across the energy gap has provided useful information about the layer width fluctuations whose characteristic dimension exceeds that of the exciton diameter. However, the direct-band-gap luminescence is an efficient process and its magnitude is relatively insensitive to small interface imperfections, particularly to effects which occur on the scale of the bulk lattice constant. It has been suggested some time ago[3] that this is not the case with cross interface recombination which is observed, e.g., in GaAs-AlAs superlattices when states derived from the bulk X point of AlAs are near degenerate in energy with states derived from the principal conduction-band valley of GaAs. Such a situation may occur either for a suitable choice of the width of GaAs and AlAs layers or when hydrostatic pressure is used to drive the states derived from the center of the Brillouin zone up towards the states associated with secondary valleys of AlAs. The level crossing turns the forbidden cross-interface recombination into an allowed one. The strength of the cross-interface luminescence then spans several orders of magnitude as the superlattice states derived from the central and secondary valleys cross.[4,5] The transitions originating from the conduction X states lying in the plane of the interface are particularly sensitive to interface disorder since they are not coupled to the zone center by the perfect superlattice potential. The strength of the cross-interface luminescence involving these states is therefore a sensitive function of disorder. Since the coupling in question connects the states derived from the bulk Brillouin-zone center with those derived from the zone edge, the characteristic dimension of the disorder that enhances this mixing is of order of the atomic separation.

In order to capture the microscopic signature of the interface via the valley-mixing effects, it is necessary to understand in some detail the relation between the luminescence spectra and the superlattice structure. In particular, the effect of interface disorder must be fully accounted for so that the realistic comparison of the level structure and optical spectra of perfect and imperfect superlattices can be made. No such account is available in the literature. Accordingly, in this study we begin by describing the method of calculation which is designed to achieve this objective. In Sec. III A we present a tutorial summary of the level ordering in perfect GaAs-AlAs superlattices. The electronic structure of these structures has been the subject of several recent theoretical studies.[6-12] The effects of symmetry and interface potential are described. This gives us an opportunity to provide a solid basis for further discussion and establish a link to a number of previous studies of valley-mixing effects. In Sec. III B we then report our results concerning structures with imperfect interfaces. We note there that our predictions concerning the effect of interface disorder on optical spectra appear to be in agreement with recent luminescence results on short-period structures.

II. CALCULATIONAL METHOD

The calculational method is based on the empirical pseudopotential approach of Jaros and co-workers.[11] The superlattice potential is constructed from spherically symmetric atomic pseudopotentials centered at the atomic positions of a perfect zinc-blende crystal. This potential is written as

$$V(\mathbf{r})=\sum_{i,\tau(i),R} V_i(\mathbf{r}-\tau(i)-\mathbf{R}) , \tag{1}$$

where i represents the different atomic species in the superlattice unit cell, $\tau(i)$ their positions within the unit cell, and $\mathbf{R}$ a real-space lattice vector of the superlattice. The calculation proceeds by expanding solutions of the superlattice Hamiltonian

$$H\Psi_{N,\mathbf{K}}=E_{N,\mathbf{K}}\Psi_{N,\mathbf{K}} \tag{2}$$

in terms of solutions of a bulk zinc-blende Hamiltonian (in this case that of GaAs),

$$H_0\phi_{n,\mathbf{k}}=E_{n,\mathbf{k}}\phi_{n,\mathbf{k}} ; \tag{3}$$

here N and n represent the band label in the superlattice

and bulk structures, respectively, and $\mathbf{K},\mathbf{k}$ the reduced wave vectors inside the superlattice and bulk Brillouin zones. This expansion is written as

$$\Psi_{N,\mathbf{K}}=\sum_{n,k} A_{N,\mathbf{K}}^{n,\mathbf{k}}\phi_{n,\mathbf{k}} , \tag{4}$$

where the $A_{N,\mathbf{K}}^{n,\mathbf{k}}$ are expansion coefficients defining the superlattice eigenvectors. The superlattice Hamiltonian is now written as

$$H=H_0+\Delta V , \tag{5}$$

where ΔV is the difference in the potential of the superlattice and the potential of the (GaAs) host material. A secular equation is set up between H and the $\phi_{n,\mathbf{k}}$ in the normal fashion, which is then solved by direct diagonalization. Spin-orbit coupling is included in the calculation directly.[11] The atomic pseudopotentials used in the calculation are obtained from zinc-blende form factors at bulk zinc-blende reciprocal-lattice vectors. These form factors are fitted so as to accurately reproduce the band structures of the constituents in the vicinity of the fundamental gaps. The superlattice calculation requires knowledge of the atomic pseudopotentials (in $\mathbf{k}$ space) at all values of the reciprocal-lattice vectors of the large unit cell. These are obtained from a functional fit between those fitted at zinc-blende bulk reciprocal-lattice vectors.

A cross section of the atomic positions in the x-y plane (parallel to the interface planes) is shown in Fig. 1. Also shown here are cross sections of the unit cells used in calculations with perfect $(\mathbf{R}_1,\mathbf{R}_2)$ and imperfect $(\mathbf{S}_1,\mathbf{S}_2)$ interfaces. Atoms lying in different atomic planes in the z direction (the growth direction) are distinguished. In the calculation assuming the perfect ordered interface the same atomic species lie at all lattice sites on a particular atomic plane parallel to the x-y plane. As there are four

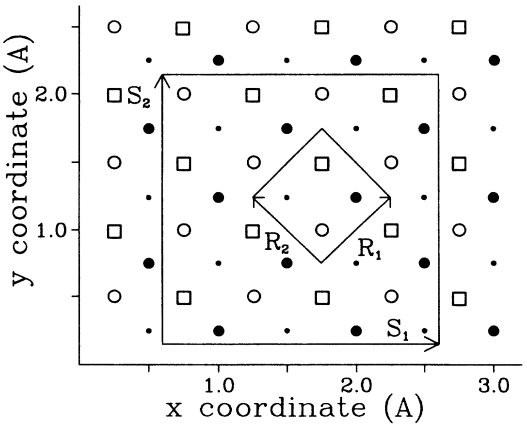

FIG. 1. Cross section of a zinc-blende lattice in the x-y plane. Different atomic layers in the z direction are represented by different symbols. Cations are represented by ●, ●, and anions by ○, □, each symbol representing a particular plane of atoms separated in the z direction. The units used are the bulk lattice constant A. The separation between adjacent atomic planes is A4 and the ordering of planes in the z direction is ●–□–●–○–●, etc. Cross sections of the unit cells associated with the ordered $(\mathbf{R}_1,\mathbf{R}_2)$ and disordered $(\mathbf{S}_1,\mathbf{S}_2)$ superlattice calculations are indicated (z is the direction of the superlattice growth).

different x-y atomic planes the whole of real space can be filled with unit cells defined by the vectors $\mathbf{R}_1$ and $\mathbf{R}_2$ ($\mathbf{R}_3$ lies in the z direction and is defined by the superlattice period). These vectors define the conventional tetragonal superlattice unit cell in real space. In order to model a disordered interface, i.e., an interface which includes, say, monolayer fluctuations at the interface plane, we need to define a larger unit cell in the x-y plane. The unit cell chosen has lattice vectors $\mathbf{S}_1$ and $\mathbf{S}_2$ ($\mathbf{S}_3$ lies in the z direction and is again defined by the superlattice period). The volume of this unit cell is eight times larger than the unit cell associated with the ordered interface. The imperfect nature of this interface is then included by exchanging one Ga atom in this unit cell adjacent to an interface with an Al atom. This exchanging of atomic species is only done at one of the two interfaces in the unit cell; see Fig. 2. The irregularity at the interface is repeated with the periodicity of the large unit cell. With the particular unit cell chosen we exchange one in eight Ga atoms adjacent to the interface for an Al atom.

Because of the different charge densities associated with GaAs and AlAs, the atomic pseudopotential associated with arsenic atoms is slightly different in the two materials. To distinguish between the two arsenic potentials we shall write As′ when describing the anion in AlAs and As when describing the anion in GaAs. At the interface plane between GaAs and AlAs lies a plane of arsenic atoms. These atoms have bonds with both Ga and Al so we shall associate them with the average potential of the As and As′ atoms which we define as As″. The different atomic species associated with the $(GaAs)_3(AlAs)_3$ superlattice are shown in Fig. 2. In previous calculations on perfect interfaces the arsenic atoms at the interface have been described by either the As or As′ potentials.[11] We shall describe the differences in the numerical results due to the choice of interface potential in Sec. III.

The bulk reduced wave vectors $\mathbf{k}$ included in the expansion of the superlattice wave vectors, Eq. (4), are determined by the periodicity of the superlattice unit cell. Only values of $\mathbf{k}$ connected to $\mathbf{K}$ by a reciprocal-lattice vector of the superlattice unit cell need be included in the expansion. These bulk states are said to be folded into the same reduced wave vector in the superlattice Brillouin zone. In this study we are concerned with (001)

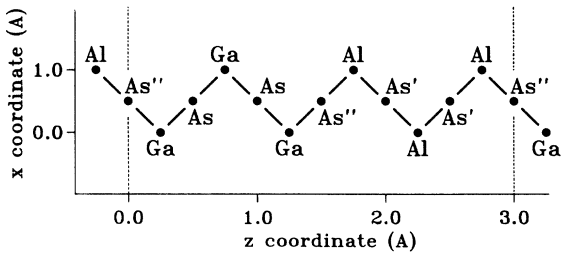

FIG. 2. Cross section of the superlattice unit cell in the x-z plane. The boundary of the unit cell in the z direction is indicated by dashed lines. The units used are the bulk lattice constant A. The different potentials associated with each atomic site are indicated. Note how three different arsenic potentials, As, As′, and As″, are used to model the superlattice.

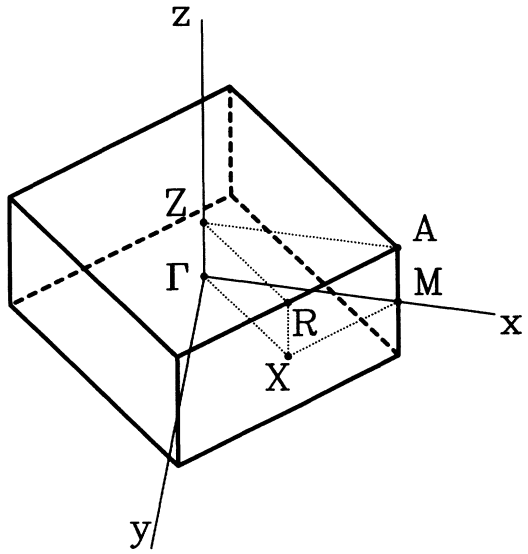

FIG. 3. Tetragonal superlattice Brillouin zone with points of symmetry indicated. The z direction is the direction of growth. The assignment of symmetry points is that due to Lax (Ref. 13).

$(GaAs)_l(AlAs)_m$ superlattices with $l+m$ even. Such superlattices have simple tetragonal symmetry and the Brillouin zone of the perfect superlattice is shown in Fig. 3 with the principal symmetry points marked.[13] The point group associated with these structures[6,7,13] is D_{2d}. In structures with perfect interfaces the bulk states folded onto a particular point in the superlattice Brillouin zone lie along a line in $\mathbf{k}$ source extending in the z direction, in the zinc-blende Brillouin zone (with suitable bulk reciprocal-lattice vector translations being made on points lying outside the bulk zone to move them inside).

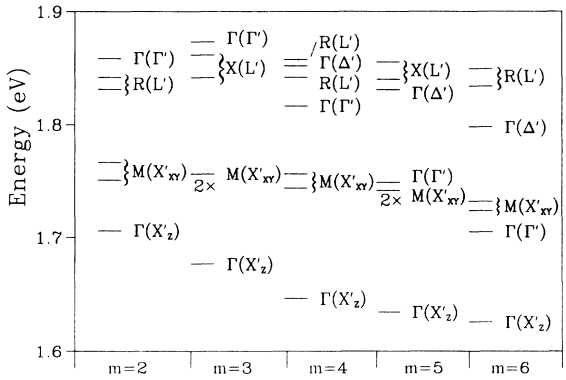

FIG. 4. Lowest conduction-band state energies in $(GaAs)_m(AlAs)_m$ superlattices with $m=1-6$. The energies are the result of calculations assuming perfect interfaces. The states are labeled according to their position in the superlattice Brillouin zone, see Fig. 3, by the undashed characters. The dashed characters in brackets represent the principal bulk minima from which the various states are derived (Δ' represents bulk states along the line Γ'-X_z' in the bulk Brillouin zone). The zero energy here is the valence-band edge in bulk GaAs. States with $2\times$ below them are doubly degenerate (without spin). With the inclusion of spin these states are split by a few meV; the energies shown here are averaged over this splitting for clarity of presentation.

In this case bulk states folded onto the same point inside the superlattice Brillouin zone are said to be coupled by the superlattice potential in the z direction. To distinguish between points of symmetry in the zinc-blende Brillouin zone and points of symmetry in the superlattice Brillouin zone we will write the zinc-blende symmetry points dashed, e.g., Γ' represents the center of the zinc-blende Brillouin zone and Γ that of the superlattice zone. For example, in structures with perfect interfaces both the bulk X_z' (001) and Γ' (000) points fold into the superlattice Γ point, but not X_x' (100), etc. When modeling the imperfect interface translational symmetry in the x-y plane is reduced and a larger unit cell is required; see Fig. 1. In this case the reciprocal-lattice vectors associated with the large unit cell are smaller in the x-y plane than those associated with the perfect interface. This means that bulk states are coupled by the superlattice potential in the x-y direction as well as the z direction. In the imperfect interface calculation states on a grid throughout the zinc-blende Brillouin zone are folded into each other. For example, the potential is now capable of coupling states from the bulk Γ', X_x', X_y', and X_z' points.

III. RESULTS

A. Perfect interface calculations

The band structure of $(GaAs)_m(AlAs)_m$ with $m=2-6$ has been calculated at the principal symmetry points in the superlattice Brillouin zone (see Fig. 3). The energy ordering of the lowest conduction-band states is displayed in Fig. 4. In the labeling of states used here the undashed letters represent the points in the superlattice Brillouin zone shown in Fig. 2 and the dashed letters in brackets indicate the bulk zinc-blende points of symmetry from which the state is mainly derived. For example, $\Gamma(X_z')$ labels a state at the center of the superlattice Brillouin zone which results from the folding in of the bulk X_z' state.

We see that in all structures considered the lowest conduction state is predicted to be the $\Gamma(X_z')$ state. The energy of the $\Gamma(X_z')$ state reduces in energy as the layer thickness increases because of a decrease in the confinement energy. This state is confirmed in the AlAs layers. In the cases where m is even the $\Gamma(X_z')$ state contains a significant amount of mixing with the bulk zone center Γ' states. In terms of the superlattice expansion, see Eq. (4), this means significant $A_{N,K}^{n,k}$ are found in this superlattice state with $\mathbf{k}=(0,0,0)$ and $(0,0,1)$, In even-m structures this mixing is allowed because states in the lowest conduction band at symmetry points X_z' and Γ' both fold onto the superlattice Γ point and result in states of the same symmetry. For example, in the $m=2$ structure the mixing of bulk states of X_z' and Γ' character results in a quasiallowed transition from the heavy-hole-like valence state to the $\Gamma(X_z')$ with a matrix element 10% of that of the allowed transition to the $\Gamma(\Gamma')$ state. In the case of m odd the folded X_z' and Γ' of the lowest conduction band result in superlattice states of different symmetry and consequently do not mix. The matrix element from the uppermost heavy-hole state to state $\Gamma(X_z')$ in this case is

much smaller than that in structures with m even. The small but finite value of the matrix element in this case results from mixing with states along the bulk Δ' line $\langle 00z \rangle$ in both states involved in the transition. At the superlattice zone center states derived from the lowest bulk Γ' conduction band are predicted to lie above those derived from the X_z' minima.

The essential physics of mixing between the lowest conduction Γ' and X' states is described by the symmetry of the two bulk eigenstates. By convention the symmetry of the electronic states in zinc-blende structures is defined relative to an origin on an anion site. The lowest zone center conduction-band state is said to have Γ_1 symmetry.[14] This state is symmetric with respect to all symmetry transformations of the group at Γ'. The symmetric nature of this state is also true for a choice of origin on a cation site. With the origin of an anion site, the lowest conduction-band state at the X_z' point is said to have X_1 symmetry. This state is symmetric with respect to all symmetric transformations of the small group at X_z'. However, if the origin is defined at a cation site, this state becomes antisymmetric with respect to symmetry transformations involving the coordinate change $z \rightarrow -z$ (i.e., with respect to the cation origin the lowest X_z' state has X_3 symmetry). The X_z' state may be represented by the function $\psi_{X_z'} = \cos(2\pi z)$, with the origin on the anion site. If the origin is changed to a cation site this function becomes $\psi_{X_z'} = \sin(2\pi z)$. The symmetry of the zone edge states as described here was used by Morgan[15] to describe radiative processes in doped semiconductors. As mentioned earlier, the degree of mixing between Γ' and X_z' states is determined by the matrix element

$$\int\int\int \psi_{\Gamma'} \Delta V \psi_{X_z'} dx\, dy\, dz \ . \tag{6}$$

When evaluating this matrix element the origin is defined at the center of the AlAs layers in the superlattice unit cell. With this choice of origin ΔV is symmetric with respect to all symmetry transformations of the superlattice. In a structure with even numbers of monolayers in each layer the center of the AlAs region is at an anion (As) site. The matrix element between the Γ' and X_z' functions with respect to this origin is written

$$\int\int\int \psi_{\Gamma'} \Delta V \cos(2\pi z) dx\, dy\, dz \ . \tag{7}$$

As this is an integral of three symmetric functions in all Cartesian directions the result is finite. Mixing between Γ' and X_z' states is allowed. In a structure with odd numbers of monolayers in each layer the center of the AlAs region is at a cation (Al) site. In this case the matrix element between Γ' and X_z' states is written

$$\int\int\int \psi_{\Gamma'} \Delta V \sin(2\pi z) dx\, dy\, dz \ . \tag{8}$$

This is an integral of an antisymmetric function in the z coordinate making the result zero. No mixing is allowed between the lowest bulk conduction Γ' and X_z' states in structures with odd numbers of monolayers in each layer.

Also shown in Fig. 4 are the states derived from the bulk X_x' and X_y' conduction-band minima. Both of these bulk minima are folded on to the superlattice M point. In the bulk these states are equivalent, i.e., both have the same energy. This equivalence in energy allows the possibility of doubly degenerate (not including spin) states resulting from the folding of these minima. The single point group associated with the M point of the superlattices considered here (D_{2d}) consists of four singly degenerate representations and one doubly degenerate representation. Whether or not the singly or doubly degenerate states are reproduced depends on the symmetry of the bulk X' states in question. If there is a finite matrix element between bulk states X_x' and X_y' and the superlattice potential ΔV, the resulting states will be mixed and split into two singly degenerate states. If the matrix element is zero, the states will not mix and the doubly degenerate representation results.

The essential physics of the splitting between the lowest conduction band X_x' and X_y' is again described by their symmetry and choice of origin. With the conventional choice of origin of an anion site, the lowest conduction-band X_x' and X_y' states are described by the functions $\psi_{X_x'} = \cos(2\pi x)$ and $\psi_{X_y'} = \cos(2\pi y)$. With the choice of origin on a cation site the X_x' and X_y' states are written $\psi_{X_x'} = \sin(2\pi x)$ and $\psi_{X_y'} = \sin(2\pi y)$. The matrix element which determines whether X_x' and X_y' mix is written

$$\int\int\int \psi_{X_x'} \Delta V \psi_{X_y'} dx\, dy\, dz \ . \tag{9}$$

We chose the origin at the center of the AlAs layers such that the potential is symmetric with respect to all symmetry transformations. In structures with even numbers of monolayers in each layer the origin is at an anion (As) site. The matrix element in this case becomes

$$\int\int\int \cos(2\pi x) \Delta V \cos(2\pi y) dx\, dy\, dz \ . \tag{10}$$

The integrand is symmetric with respect to all coordinates making the integral finite. The finite matrix element means mixing between the lowest conduction X_x' and X_y' states is allowed. The resulting states are split into two singly degenerate (without spin) states. In structures with odd numbers of monolayers in each layer the origin is at a cation (Al) site. The matrix element in this case becomes

$$\int\int\int \sin(2\pi x) \Delta V \sin(2\pi y) dx\, dy\, dz \ . \tag{11}$$

The integrand is antisymmetric with respect to both x and y coordinates, making the integral zero. This means no mixing is allowed between the lowest conduction X_x' and X_y' states in structures with odd numbers of monolayers in each layer. In these structures the doubly degenerate states (without spin) result.

The doubly and singly degenerate states described above are shown in Fig. 4. We point out here that the energy levels in Fig. 4 are averaged over spin. A group-theoretical analysis using the double (spin) group predicts only doubly (spin) degenerate representations at the superlattice M point.[16] This result is returned in our calculation. The doubly degenerate states in Fig. 4 represent, with spin, four single-electron states. They are in fact split into two spin-degenerate pairs, the splitting being a few meV in the periods considered here. These splittings

are not shown for clarity of presentation. If we examine the lowest $M(X_x',X_y')$ states derived from the lowest conduction band, we find doubly degenerate states result with m odd and singly degenerate states result with m even. The results here appear to contradict those of previous calculations using the same method.[7] The contradiction arises because of the choice of potential at the interface arsenic atomic sites. In Ref. 17 one interface potential was assigned the potential associated with As and the other was assigned the potential associated with As'. This assignment results in a different point group for the superlattice and consequently different symmetry splitting of the states. The physically correct picture is to assign the same averaged, As'', potential at both interfaces as is done here. With this choice of potential the ordering of the single and double degeneracies agrees with other calculations on similar structures.[6,7]

It is appropriate at this point to discuss the sensitivity of the results to the choice of interface potential. In the calculation described above the arsenic at the interface plane (As'') was chosen to have the average atomic pseudopotential of those associated with AlAs (As) and GaAs (As'). If instead we were to place As' (or As) atoms at each interface plane, retaining the D_{2d} space group of the superlattice, the splitting of the lowest X_x' and X_y' states is considerably increased. In the $(GaAs)_2(AlAs)_2$ structure placing As' atoms at both interfaces resulted in a splitting of 130 meV. Alternatively, it is possible to fit the form factors at the bulk reciprocal-lattice vectors to achieve the same anion atomic potential in both materials. There is now no question as to what potential to associate with the interface. With this limitation in the scope for fitting the form factors accurate bulk band structures can be achieved in the vicinity of the fundamental gap, but at the expense of the accuracy of states away from this region. Such an approach in the $m=2$ case returns a value of the splitting of X_x'-X_y' of 3 meV. Because of the different charge densities in GaAs and AlAs, we expect a slightly different atomic pseudopotential associated with arsenic in the two different compounds. As the arsenic atom at the interface is bonded to both Al and Ga, we chose the average As'' potential at the interface. This approach returns a splitting of 20 meV, in quantitative agreement with other estimates of this energy splitting.[6,7] The choice of interface potential is not so important in large-period structures. In structures with $m\sim 10$ different choices of the interface potential result in changes in energies of only a few meV. This is because the interface potential is only a small fraction of the total potential. States derived from the bulk L' minima are also shown in Fig. 4. In superlattices with m even the bulk L' minima fold onto the superlattice X point, see Fig. 3. In superlattices with m odd and bulk L' minima fold onto the superlattice R point. All states derived from the L' minima are predicted to lie above those derived from the bulk X' minima.

The effect of strain has not been accounted for in the calculations reported here. The lattice constant of AlAs is 0.14% larger than that of GaAs. With superlattices grown on GaAs substrates the AlAs layers are subjected to a compression in the x-y plane due to this small lattice mismatch. In this strain configuration the bulk X_z' states of AlAs are pushed up by 23 meV above the X_x' and X_y' bulk states.[18] As the lowest superlattice states derived from these minima are confined in the AlAs layers, similar energy shifts of the $\Gamma(X_z')$ relative to the $M(X_x',X_y')$ states are expected. These strain-induced energy shifts need to be considered to predict the energy ordering of the lowest superlattice conduction states. A qualitative description of the factors which determine the energy ordering of the conduction-band states is obtained from an effective-mass picture. The electron states are described by a particle with the relevant effective mass confined in regular potential wells defined by the band offset. The energy ordering of the states is determined by their confinement energy and the strain-induced splitting. The confinement energy of the $M(X_x',X_y')$ states in the direction of growth is determined by the transverse effective mass m_T^*. This effective mass is smaller than that longitudinal effective mass m_L^*, which determines the confinement energy of the $\Gamma(X_z')$ state. This means the confinement energy associated with the $M(X_x',X_y')$ states is larger than that associated with the $\Gamma(X_z')$ state. Considering only confinement energy the $M(X_x',X_y')$ states lie above the $\Gamma(X_z')$ states in all structures considered; see Fig. 4. Including the strain correction the $\Gamma(X_z')$ state is pushed up in energy relative to the $M(X_x',X_y')$ states. For the values of m considered, the $\Gamma(X_z')$ state is still predicted to be the lowest conduction-band state. Only in the limit of very large well widths ($m\sim 20$), when confinement energy of all states is small, is $M(X_x',X_y')$ predicted to be lower in energy than $\Gamma(X_z')$ due to the strain splitting of the bulk X' minima.

B. Imperfect interface calculations

We have modeled two different superlattice structures incorporating monolayer imperfection at the interface as described in Sec. II. These structures are $(GaAs)_{12}(AlAs)_8$ and $(GaAs)_3(AlAs)_3$. In the $(GaAs)_{12}(AlAs)_8$ structure the imperfect interface was repeated with the periodicity of the superlattice in the direction of growth. In the $(GaAs)_3(AlAs)_3$ structure the disordered interface was repeated with twice the periodicity of the superlattice in the direction of growth, i.e., the large unit cell was twice as long as that of the superlattice with the ordered interfaces. The monolayer fluctuation is incorporated into one of the four interfaces in this cell. In particular in these structures we wish to highlight the role of interface disorder in affecting the degree of momentum mixing between the lowest Γ'-like and X'-like conduction-band states. In the large unit cell used to model the imperfect interface, bulk states from Γ', X_x', X_y', X_z', and L' are all connected to each other by reciprocal-lattice vectors of the large unit cell, i.e., mixing between all of these bulk states is allowed, due to the reduced symmetry in the x-y plane. Because of the similarity in the atomic pseudopotentials of Ga and Al the degree of interface imperfection required to produce a significant change in the electronic and optical properties of these structures was found to be at least one in eight

cations at the cation interface planes exchanged. This is the degree of disorder modeled in this study.

First, we shall consider the $(GaAs)_{12}(AlAs)_8$ structure. It has been shown experimentally[19] and theoretically[20] that, at atmospheric pressure, this structure exhibits near degeneracy of the lowest Γ'- and X'-like states. In Fig. 5 we show the variation in the momentum matrix elements between the uppermost heavy-hole-like state and lowermost X'- and Γ'-like conduction states as a function of the separation between these conduction states $\Delta E_{\Gamma,X}$. The strength of the matrix element is an indication of the amount of Γ' character present in each conduction state. An allowed transition to the heavy-hole subband requires a significant amount of the wave function to be derived from the Γ' conduction state. The change in energy separation between Γ' and X' and consequently a change in momentum mixing can be achieved by varying the pressure on the superlattice. An increase in pressure pushes the Γ' state up in energy relative to the X' states. At a value of $\Delta E_{\Gamma,X_z}$ of 5 meV the momentum matrix elements are comparable as each state contains a significant amount of the Γ' character required for an allowed transition. As the separation $\Delta E_{\Gamma,X_z}$ is increased, the matrix element to the Γ' state increases at the expense of that to the X_z' state as the amount of mixing decreases. The corresponding matrix elements to the X_x' and X_y' states at similar energy separations are not shown in this figure as they are very small in comparison ($\leq 10^{-4}$ a.u.), i.e., the amount of Γ' character in these states is very small. A summary of the absolute values of the matrix elements across the gap is shown in Table I. These results are only 2% different from those obtained in a calculation on the equivalent perfect interface superlattice. The matrix element to the X_z' state is 2% less in the imperfect interface case as compared to the perfect interface case. We find that the small differences between the ordered and disordered results are due to the relatively large period of superlattice under consideration. In this case the interface potential associated with the disorder only represents a small fraction of the total superlattice potential.

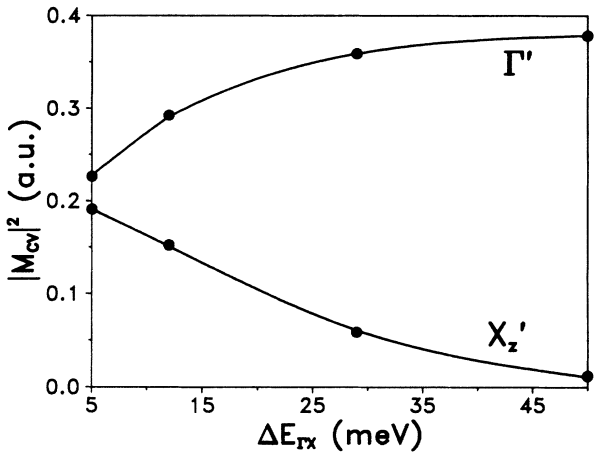

FIG. 5. Squared across gap mixture element $|M_{CV}|^2$ between the Γ'- and X_z'-like lowermost conduction states and the uppermost heavy-hole state in the $(GaAs)_{12}(AlAs)_8$ superlattice. These are results of calculations including monolayer imperfections at the interface. The matrix element is plotted as a function of the separation between the Γ'- and X'-like conduction states $\Delta E_{\Gamma X}$. This energy separation may be varied by changing the pressure on the structure. The matrix element to the $(X_x'$-$X_y')$-like state is not shown as it is not discernible on the scale of the figure.

TABLE I. Summary of the squared optical matrix elements between the uppermost heavy-hole-like state and the Γ'- and X'-like conduction-band states in the $(GaAs)_{12}(AlAs)_8$ and $(GaAs)_3(AlAs)_3$ structures, as a function of the separation between the Γ'- and X'-like states. The units of the matrix elements are atomic units. Results for both X_z'- and $(X_x'$-$X_y')$-like states are shown.

$\Delta_{\Gamma X}$ (meV)	10	20	30	40
$\Gamma'(12,8)$	0.275	0.332	0.360	0.376
$X_z'(12,8)$	0.161	0.103	0.056	0.028
X_x'-$X_y'(12,8)$		4×10^{-4}		
$\Gamma'(3,3)$	0.313	0.360	0.386	0.390
$X_z'(3,3)$	0.078	0.035	0.011	0.002
X_x'-$X_y'(3,3)$		0.040	0.014	0.004

We have also calculated the decay time across the superlattice band gap from the X_z'-like state. With the inclusion of the average interface potentials described in Sec. III we find significant changes in the absolute value of this decay time compared to previous calculations where As' atoms were placed at each interface.[20] For example, we find that for a value of $\Delta E_{\Gamma,X_z}$ of 30 meV the calculated decay time in this structure is 1.5 μs. The calculated decay time becomes longer than the observed decay time by about an order of magnitude. The measured decay time is that between excitonic states. No account of excitonic effects has been made in this study. The increased transition strength between excitonic states compared to that between free states accounts for the difference between the measured and predicted decay times. However, the change due to this choice of potential in the quasilinear dependence of the decay time upon Δ_{Γ,X_z} is only 2%. Consequently, our previous conclusions (Fig. 2 of Ref. 20) remain unchanged.

We shall now consider the $(GaAs)_3(AlAs)_3$ superlattice. As previously stated only one interface in four has the monolayer imperfection incorporated into it. The energies of the lowest conduction states as a function of pressure are shown in Fig. 6. It should be noted that although all states contain significant contributions from all bulk minima, they are labeled according to the most dominant contribution. We find that the band structure at atmospheric pressure is significantly different from that calculated in the perfect interface calculation; see Fig. 4. The splitting between the X_z' and X_x'-X_y' derived states is reduced by 50 meV in going from the perfect to imperfect case and the Γ' derived state is significantly reduced in energy.

In Fig. 7 we plot the momentum matrix elements from the highest heavy-hole-like state to the Γ' and X' derived

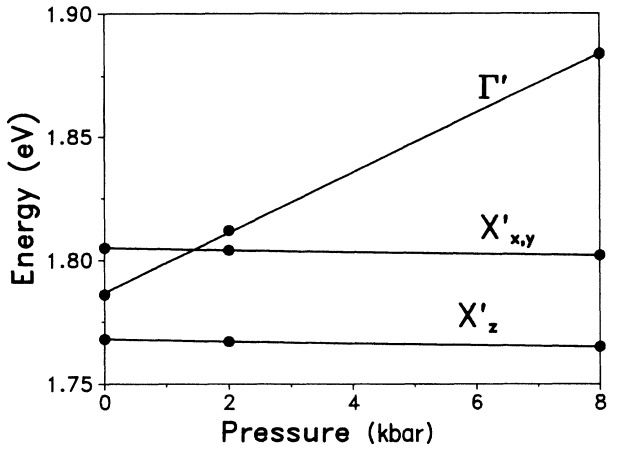

FIG. 6. Energy of the lowest Γ'- and X'-like conduction states, in the $(GaAs)_3(AlAs)_3$ structure, as a function of pressure. These are results of calculations including monolayer imperfections at the interface. These energies are without the strain correction. With the strain correction the X_x'-X_y' and X_z' states are expected to lie very close in energy.

conduction states as a function of the separation $\Delta E_{\Gamma,X}$. This variation in energy separation is achieved by changes in pressure as shown in Fig. 6. Since disorder changes $\Delta E_{\Gamma,X}$, this provides a good measure of the sensitivity of the optical spectra to disorder. The momentum matrix elements are calculated to both the X_z' and X_x'-X_y' derived conduction states. We find that the largest momentum matrix element to the X_z'-like state is significantly smaller than that in the $(GaAs)_{12}(AlAs)_8$ structure at comparable values of $\Delta E_{\Gamma,X_z}$. This is well accounted for by the symmetry argument presented in Sec. III A since this superlattice has odd numbers of monolayers in each layer. The value of this matrix element is 7% less in the imperfect interface calculations as compared to the perfect case. However, the matrix elements to the X_x'-X_y' states shown in Fig. 7 are significantly larger than those in the $(GaAs)_{12}(AlAs)_8$ case at similar values of $\Delta E_{\Gamma,X_{xy}}$. This transition is identically zero (forbidden) in the perfect interface calculation. The relatively large value of this matrix element in the $(GaAs)_3(AlAs)_3$ is due to the increased importance of the interface potential as a fraction of the total superlattice potential in this smaller-period case. This increased importance of the disordered interface in the smaller period case also accounts for the greater change in band structure between the perfect and imperfect calculations. A summary of the momentum matrix elements across the gap in these two structures is presented in Table I. The values of the optical matrix elements are given versus the magnitude of the $\Delta E_{\Gamma,X}$. This is the best measure of the valley mixing since the strength of any effect such as disorder, pressure, or chemical composition can be reduced to it.

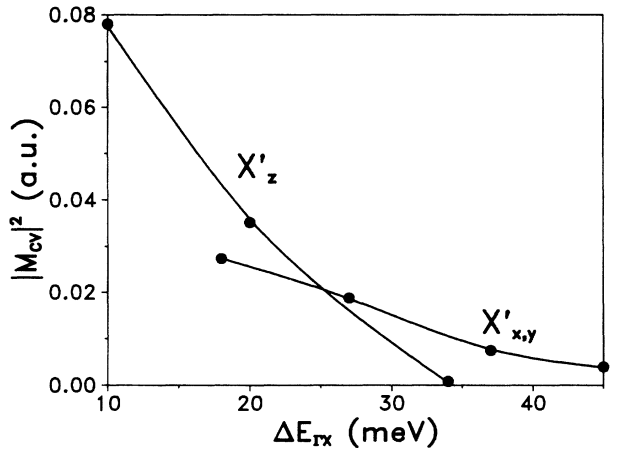

FIG. 7. Plot of $|M_{CV}|^2$ (see Fig. 5) against the separation of the Γ'-like and X' states, $\Delta E_{\Gamma X}$, in the $(GaAs)_3(AlAs)_3$ structure. These are results of calculations including monolayer imperfections at the interface. Results for the matrix element to both the X_z'-like and $(X_x'$-$X_y')$-like states are shown. The transition to the $(X_x'$-$X_y')$-like state is made allowed by the interface disorder.

With the inclusion of strain as described in Sec. III A, the X_z'-like state in the three-monolayer structure will be pushed up in energy to within 10 meV of the $(X_x'$-$X_y')$-like state. The Γ'-like state is also pushed up in energy. It is therefore possible, given the calculational uncertainties, that the lowest conduction state is the X_x'-X_y' state in agreement with the experimental results of Ge *et al.*[2] Also of interest here is the strength of the transition to the X_x'-X_y' state. We predict a transition strength a few percent of that associated with a direct transition. This is in close agreement with the results of Ge and coworkers.[21] This suggests first of all that the degree of disorder assumed in our model is about the same as that in the sample studied by Ge *et al.* It also suggests that given a wider set of data, which would permit a more thorough test of the absolute values generated in our calculations, theory might be in a position to achieve an accurate characterization of the microscopic signature of semiconductor interfaces. It is clear from our Table I that a small difference in energy separation $\Delta E_{\Gamma,X}$ induced by disorder leads to significant changes in valley mixing. This is a good measure of the sensitivity of our interface "probe." One could simply tabulate the strength of the optical matrix element versus the percentage of atoms transferred across the interface. For example, if we changed the number of transferred atoms from 1 in 8 to 1 in 16, the predicted optical matrix element would change by nearly an order of magnitude.

We have also performed calculations on structures where the symmetry of the perfect superlattice is preserved and imperfections at the interface is represented by weighting the potential associated with the Ga and Al atoms adjacent to one of the interfaces. To model the imperfect interface situation where one in eight cations adjacent to an interface is swapped, the new (average) potential associated with the cation on the GaAs side of the interface is given by $V=\frac{7}{8}V(\mathrm{Ga})+\frac{1}{8}V(\mathrm{Al})$. This modeling has been done for both structures presented in this section. We find that the energy of the lowest conduction-band states remains unchanged to within a

few meV. This result is explained by the delocalized nature of the states in the imperfect interface calculation in the plane of the interface. Because each state shows no particular localization to the imperfect interface sites, each state sees the "average" potential parallel to each interface plane as modeled above. However, this simpler calculation cannot predict the strengths of transitions to the $(X_x'$-$X_y')$-like states as no mixing of states in the plane of the interface can be produced by this approach.

IV. SUMMARY AND CONCLUSIONS

We have reported the first quantitative assessment of the effect of microscopic disorder upon optical spectra of GaAs-AlAs superlattices. We concentrated on optical transitions between states derived from the AlAs X' minima in the barriers and those derived from the top of the valence band located in GaAs wells. The strength of the optical spectra depends on the degree of coupling by the crystal potential of the states derived from the bulk Brillouin-zone center (Γ') and those from the edge (X') along the cubic axes. In short-period superlattices such as $(GaAs)_3(AlAs)_3$ with perfect interfaces, the lowest level is always that associated with the X' states lying along the growth axis (z). The effect of disorder—which we model by a swap of every eight Ga and Al atoms in the interface monolayers—is to alter radically the separation of X'-like states. As a result the states lying perpendicular to the interface plane are pushed up in energy and if the effect of the strain is included they are predicted to be separated from those parallel to the interface only by about 10 meV. The calculated optical transition from the X' states in the interface plane to the valence band becomes large and for this degree of disorder compares well with the available experimental value. We show that the optical strength is a sensitive function of the degree of disorder, which is usefully measured by the degree of disorder-induced change in the separation of the states Γ' and X_x', X_y' and X_z' character obtained for the perfect structure. The predicted Γ'-X' separation can be measured by the application of hydrostatic pressure and provides a useful tool for testing our theory. The changes in the optical strength for the zone-folded levels oriented along the growth axis also scale with the separation of the X'- and Γ'-like states. In larger-period structures the effect of disorder upon the optical spectra is reduced but remains observable. This is demonstrated for the model disorder employed here for wells and barriers containing about ten monolayers each. Our results show that cross-interface recombination can be used as a sensitive probe for microscopic characterization of semiconductor interfaces.

ACKNOWLEDGMENTS

We are grateful to L. J. Sham, and Y. T. Lu for stimulating correspondence. Also, we would like to thank the Science and Engineering Research Council (United Kingdom), the Procurement Executive (Ministry of Defence) Royal Signals and Radar Establishment, Malvern, and the U.S. Office of Naval Research (ONR) and ONR Contract No. N00014-88-J-100 for financial support.

[1]A. Ishibashi, Y. Mori, M. Itabashi, and M. Watanabe, J. Appl. Phys. **58**, 2691 (1985).
[2]W. Ge, M. D. Sturge, W. D. Schmitt, L. N. Pfeiffer, and K. W. West, Appl. Phys. Lett. **57**, 55 (1990).
[3]M. Jaros, Rep. Prog. Phys. **48**, 1091 (1985).
[4]D. J. Wolford, T. F. Keuch, J. A. Bradley, M. A. Gell, D. Ninno, and M. Jaros, J. Vac. Sci. Technol. B **4**, 1043 (1986).
[5]M. A. Gell, D. Ninno, M. Jaros, D. J. Wolford, T. F. Keuch, and J. A. Bradley, Phys. Rev. B **35**, 1196 (1987).
[6]Y. T. Lu and L. J. Sham, Phys. Rev. B **40**, 5567 (1989).
[7]S. H. Wei and A. Zunger, J. Appl. Phys. **63**, 5794 (1988).
[8]B. M. Bylander and L. Kleinman, Phys. Rev. B **34**, 5280 (1986).
[9]S. B. Zhang, M. S. Hybertsen, M. L. Cohen, S. G. Louie, and D. Tomanek, Phys. Rev. Lett. **63**, 1495 (1989).
[10]H. W. van Kesteren, E. C. Cosman, P. Dawson, and C. T. Foxon, Phys. Rev. B **39**, 13 426 (1989).
[11]M. A. Gell, D. Ninno, M. Jaros, and D. C. Herbert, Phys. Rev. B **34**, 2416 (1989).
[12]J. S. Nelson, C. Y. Fong, and I. P. Batra, Appl. Phys. Lett. **50**, 1595 (1987).
[13]M. Lax, *Symmetry Principles in the Solid State and Molecular Physics* (Wiley, New York, 1974).
[14]R. H. Parmenter, Phys. Rev. **100**, 573 (1955).
[15]T. N. Morgan, Phys. Rev. Lett. **21**, 819 (1968).
[16]J. F. Cornwell, *Group Theory and Electronic Energy Bands in Solids* (North-Holland, Amsterdam, 1969).
[17]L. D. L. Brown, M.Jaros, and D. J. Wolford, Phys. Rev. B **40**, 6413 (1989).
[18]P. Dawson, C. T. Foxon, and H. W. van Kesteren, Semicond. Sci. Technol. **5**, 54 (1990).
[19]M. S. Skolnick, G. W. Smith, I. L. Spain, C. R. Whitehouse, D. C. Herbert, D. M. Whittaker, and L. J. Reed, Phys. Rev. B **39**, 11 191 (1989).
[20]L. D. L. Brown and M.Jaros, Phys. Rev. B **40**, 10 625 (1989).
[21]W. Ge (private communication).